POLITECNICO DI TORINO
Repository ISTITUZIONALE

Exploring Novel Transmission Mechanisms for Rotary Electromagnetic Shock Absorbers

*Original*
Exploring Novel Transmission Mechanisms for Rotary Electromagnetic Shock Absorbers / Moscone, G., Bisciaio, G., Sorrentino, G., Zhang, X., Galluzzi, R., Amati, N.. - In: ENGINEERING PROCEEDINGS. - ISSN 2673-4591. - ELETTRONICO. - 131:1(2026). [10.3390/engproc2026131021]

*Availability:*
This version is available at: 11583/3009648 since: 2026-04-07T11:59:05Z

*Publisher:*
MDPI

*Published*
DOI:10.3390/engproc2026131021

*Terms of use:*

This article is made available under terms and conditions as specified in the corresponding bibliographic description in the repository

*Publisher copyright*

(Article begins on next page)

27 November 2026

engineering proceedings

*Proceeding Paper*

# Exploring Novel Transmission Mechanisms for Rotary Electromagnetic Shock Absorbers †

**Giulia Moscone [1,2], Giorgio Bisciaio [1,2,*], Gennaro Sorrentino [1,2], Xinyan Zhang [1,2], Renato Galluzzi [3,*] and Nicola Amati [1,2]**

[1] Department of Mechanical and Aerospace Engineering, Politecnico di Torino, 10129 Turin, Italy; giulia.moscone@polito.it (G.M.); gennaro.sorrentino@polito.it (G.S.); xinyan.zhang@polito.it (X.Z.); nicola.amati@polito.it (N.A.)
[2] Center of Automotive Research and Sustainable Mobility, Politecnico di Torino, 10129 Turin, Italy
[3] School of Engineering and Sciences, Tecnologico de Monterrey, Mexico City 14380, Mexico
* Correspondence: giorgio.bisciaio@polito.it (G.B.); renato.galluzzi@tec.mx (R.G.)
† Presented at the 54th Conference of the Italian Scientific Society of Mechanical Engineering Design (AIAS 2025), Florence, Italy, 3–6 September 2025.

**Abstract**

Active suspension systems are gaining growing attention in the automotive industry. This trend aligns with vehicle electrification and X-by-wire technologies adoption, also answering to the increasingly stringent requirements for passenger comfort and safety. Among the possible solutions, electromechanical actuators represent a valid alternative to traditional shock absorbers, integrating an electric machine that can be easily controlled to deliver the desired forces in both active and passive operations. The present work aims at developing an innovative transmission compound for a rotary electromagnetic active suspension system that is able to obtain high level NVH and safety performances. Two different proposed systems are analyzed. The first one couples a cycloidal transmission stage to a polymeric planetary one, while the second one couples the same cycloidal stage to a concentric magnetic gearbox. Both of them are expected to improve the NVH performances of the shock absorber, thanks to the high efficiency of the cycloidal reducer and to the properties of plastic materials and of magnetic coupling. The proposed systems are analyzed analytically and in simulation environment, providing promising results in terms of efficiency and torque density.

**Keywords:** active damper; actuator; electromechanical; gearbox; shock absorber

Check for updates

Academic Editors: Nicola Bonora, Umberto Galietti, Luigi Bruno, Davide Castagnetti, Cristiana Del Prete, Mario Guagliano and Vigilio Fontanari

Published: 31 March 2026

**Copyright:** © 2026 by the authors. Licensee MDPI, Basel, Switzerland. This article is an open access article distributed under the terms and conditions of the Creative Commons Attribution (CC BY) license.

## 1. Introduction

Active vehicle suspensions represent one of the streamlines towards electrification in the automotive industry. The integration of mechatronic chassis actuators is a crucial step in guaranteeing optimal comfort and handling performances at the vehicle level. Electric vehicles impose more stringent requirements in terms of vertical dynamics due to the inclusion of a battery pack. Because of the removal of the internal combustion engine, electric vehicles also demand lower levels of noise coming from road irregularities. Comfort and noise, vibration and harshness (NVH) are even more relevant in the context of autonomous vehicles, where the driver could become more susceptible to external disturbances. In this context, the possibility of exerting force directly at the shock absorber level becomes extremely attractive.

Among all the possible proposed systems, electromechanical actuators represent an interesting solution thanks to their reduced inertia when compared to hydraulic solutions, their oil-free nature, high efficiency, and the possibility of energy harvesting from road unevenness [1]. In these actuation systems, rotary electric motors are preferred over linear ones due to their higher torque and power density [2]. Therefore, the actuator requires a suitable transmission mechanism to convert rotation into the linear displacement, typical of a vehicle suspension, while also providing a speed reduction. An industrial example of a rotary shock absorber, connected to the suspension by linkages and able to regenerate power is the novel concept proposed by Audi AG in 2016, with the eROT system [3].

Previous studies in our research group have led to the development of rotary actuation technologies for suspensions, where an electric machine coupled to a speed reducer drives a lever system, thus providing linear actuation to the suspension arms [4]. This setup has led to favorable results in terms of packaging, efficiency, responsiveness and output force. However, the design of the speed reducer can still be addressed to enhance the system characteristics. This component is indeed a crucial part of the actuator as it must deliver high reduction ratios, usually higher than 50:1, in a limited torque-speed envelope.

In previous prototypes, this has led to the development of a double-stage planetary gearbox with low-module spur gears, developing a total reduction ratio $i_{tot} = 87$. This design can deliver favorable performance and compactness. However, it also presents drawbacks in terms of cost and mechanical issues, such as wear and backlash. The latter, together with static transmission error and gear meshing frequencies, also leads to poor NVH performance of the actuator [5]. Specifically, these issues add a source of noise particularly related to the high-speed stage.

To address these drawbacks, this research aims at proposing innovative compound transmissions. Cycloidal drives present several benefits for acoustic behavior, reducing backlash and vibrations, while still providing high transmission ratios in a compact size. However, using a single stage with a high reduction ratio can affect the overall system efficiency [6]. Therefore, double stage compound gearboxes are proposed. Starting from the benchmark planetary gearbox, the low-speed stage is replaced by a cycloidal drive, while two possible alternatives are investigated for the high-speed stage. The first consists of a contactless magnetic drive [7]. The contact-free nature of the magnetic gears improves durability and minimizes component wear, contributing to a more efficient and low-maintenance solution. Leveraging the intrinsic properties of magnetic coupling, the system could provide a fail-safe mechanism, enabling torque decoupling when the applied torque exceeds the design limits. This feature helps prevent mechanical failure of other components in limit conditions, thus improving system reliability. The second alternative introduces a high-strength polymer planetary stage. This solution is expected to be extremely cost-effective, while also obtaining a strong noise reduction thanks to the adoption of a material with more intrinsic damping.

This work provides a feasibility study for these novel compound gearboxes. Both solutions are compared against the steel planetary benchmark, in terms of efficiency and packaging. The sequel of this manuscript is organized as follows. Section 2 describes the initial design steps to determine the requirements for each transmission stage. In Section 3, the cycloidal stage design is performed through an optimization process. Once the low-speed stage is defined, both planetary and magnetic stages are designed respectively in Sections 4 and 5. The latter is, again, the result of an optimization-driven approach, while the polymer planetary stage is designed with traditional software tools. Finally, Section 6 concludes this work.

https://doi.org/10.3390/engproc2026131021

## 2. Transmission Sizing

As previously explained in Section 1, the gearbox design is crucial to reduce noise and vibrations of the actuator while maintaining a fair conversion efficiency of the system. In contrast with the benchmark double-stage planetary reducer, the aim is to attain a more favorable compromise between NVH and conversion efficiency. This is achieved with a cycloidal first stage and a second high-speed stage with magnetic or polymer gears. Both high-speed stage configurations share the same cycloidal first stage, which implies a shared reduction ratio among both solutions.

Single stage planetary reducers with a fixed ring can reach practical gear ratios from 3:1 to 9:1 [8]. Higher or lower ratios lead to an unbalance of gear geometry, respectively with too small sun or planets, compromising their mechanical strength. Indeed, the best ratios for maximized torque capability are usually considered to be between 4:1 and 6:1 [9].

Conversely, the magnetic stage ratio limitations are strictly related to the achievable number of magnetic poles on inner and outer rotors, as described in Section Magnetic Stage Design Results and Equation (5). Note that, the higher the number of pole pairs in the inner rotor, the better the torque ripple performance [10]. Due to permanent magnets size and envelope constraints, the maximum number of external pole pairs is set to 15. In this specific case, a number of inner rotor pole pairs of 3 is selected, as a higher number would yield excessively low transmission ratios. Also, to maintain fair torque ripple performance [11], no integer reduction ratio should be adopted, reducing the acceptable outer rotor pole pairs to 14. Applying Equation (5), the magnetic stage ratio can reach up to 4.66, with steps of 0.33 due to the three internal pole pairs.

Combining the limitations of the two technologies, the final acceptable range for the high-speed stage is obtained:

$$\begin{aligned} i_{st2} &\in [3, 9] \quad \text{Planetary constraint} \\ i_{st2} &\leq 4.66 \quad \text{Magnetic constraint} \\ \therefore\ i_{st2} &\in \{3.33, 3.66, 4.33, 4.66\} \end{aligned} \tag{1}$$

where $i_{st2}$ is the fast stage ratio. Since the total gearbox reduction ratio is fixed to match the previous solutions with $i_{tot} = 87$, the acceptable range for the cycloidal stage ratio $i_{cyc}$ can be calculated:

$$\begin{aligned} i_{cyc} &= \frac{i_{tot}}{i_{st2}} \\ i_{cyc} &\in \mathbb{N}^{+} \\ \therefore\ i_{cyc} &\in \{19, 20, 24, 26\} \end{aligned} \tag{2}$$

The envelope constraints for all three reducers are set to a maximum diameter of 90 mm and an active axial length of 20 mm to ensure a compact design of the actuator as similar as possible to the original planetary prototype.

## 3. Cycloidal Drive

A cycloidal drive is an alternative speed reducer, often employed in robotics [12,13], which exploits the rotation of usually two eccentric cycloidal disks on fixed external pins to transmit torque to the slower output shaft, connected through the output holes. This concept is illustrated in Figure 1.

The proposed design approach is based on a multibody analysis developed in MATLAB®. Once the geometric and material parameters are selected, the model yields the contact forces between the disks, pins, and rollers, which are used to calculate the stresses

and size the various components. It also yields friction forces, which are useful to obtain a first estimation of the reducer's efficiency.

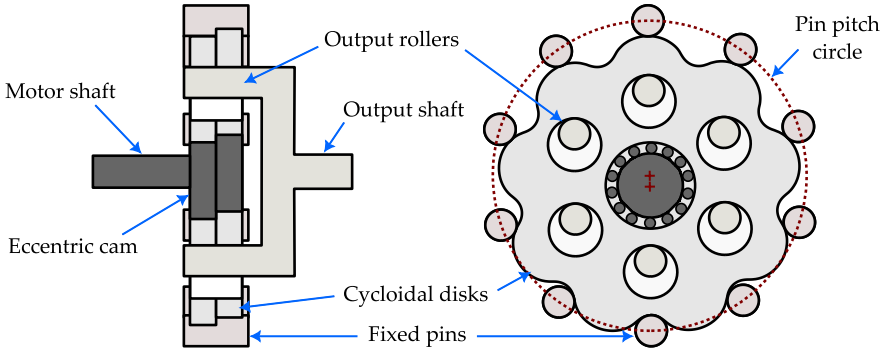


**Figure 1.** Cycloidal drive and its main components.

### *3.1. Optimized Cycloidal Stage Design*

The design of the cycloidal drive is performed through an optimization process to define all the geometrical parameters.

The main design requirements for the cycloidal stage are summarized in Table 1. The reduction ratios allowed for the cycloidal stage are obtained from Equation (2). The maximum thickness of the disk is given by the half of the maximum active length for the entire cycloidal stage (20 mm), as two disks are adopted to balance eccentric forces [14]. The pitch diameter of the external pins is also varied in the optimization process, still satisfying the envelope constraint of 90 mm. A common minimum safety factor is set to 1.2 for all components sizing.

**Table 1.** Cycloidal drive design requirements.

| Description | Symbol | Value | Unit |
|---|---|---|---|
| Required transmission ratio | $i_{cyc}$ | 19, 20, 24, 26 | – |
| Disk maximum thickness | $t_{max}$ | 10 | mm |
| Fixed pins pitch diameter | $D$ | 80 to 90 | mm |
| Minimum Safety factor | $SF_{min}$ | 1.2 | – |

First, the disk profile design is optimized, studying the effect on system efficiency due to pins' pitch diameter $D$, eccentricity $E$, and reduction ratio $i_{cyc}$.

The pin radius $R_p$ for each $D$, $E$, and $i_{cyc}$ combination is maximized, since it was observed that a larger pin radius leads to higher efficiency. Its upper boundary $R_{p\,max}$ is given by interference and undercut constraints [15] as given by the Equation (3).

$$R_{p\,max} = \min \begin{cases} R \sin\left(\dfrac{\pi}{N}\right) & \text{interference} \\ \sqrt{\dfrac{27n(R^2 - E^2N^2)}{(n+2)^3}} & \text{undercut} \end{cases} \tag{3}$$

where $R$ is the pitch radius of the pins, equal to $D/2$, $N$ is the number of external pins, while $n$ is the number of disk lobes. Both are bound to the reduction ratio given by Equation (4). To maximize the gear ratio $N - n$ is kept equal to 1.

$$i_{cyc} = \frac{n}{N - n} \tag{4}$$

The output torque is kept constant throughout optimization, varying the input torque in function of $i_{cyc}$.

Together with the system efficiency, as shown in Figure 2a, the minimum required disk thickness is also computed, as shown in Figure 2b. Hertz theory is applied to compute the stresses in the contact points between fixed pins and disk, and the minimum thickness $t_{Hz,pin}$ is computed to satisfy the requirement of $SF_{min} = 1.2$. All solutions with a $t_{Hz,pin} > 10\,mm$ are rejected, and between the compliant solutions, as shown in Figure 2c, the most efficient is selected. Finally, in Figure 2d, the adopted pin radius is indicated.

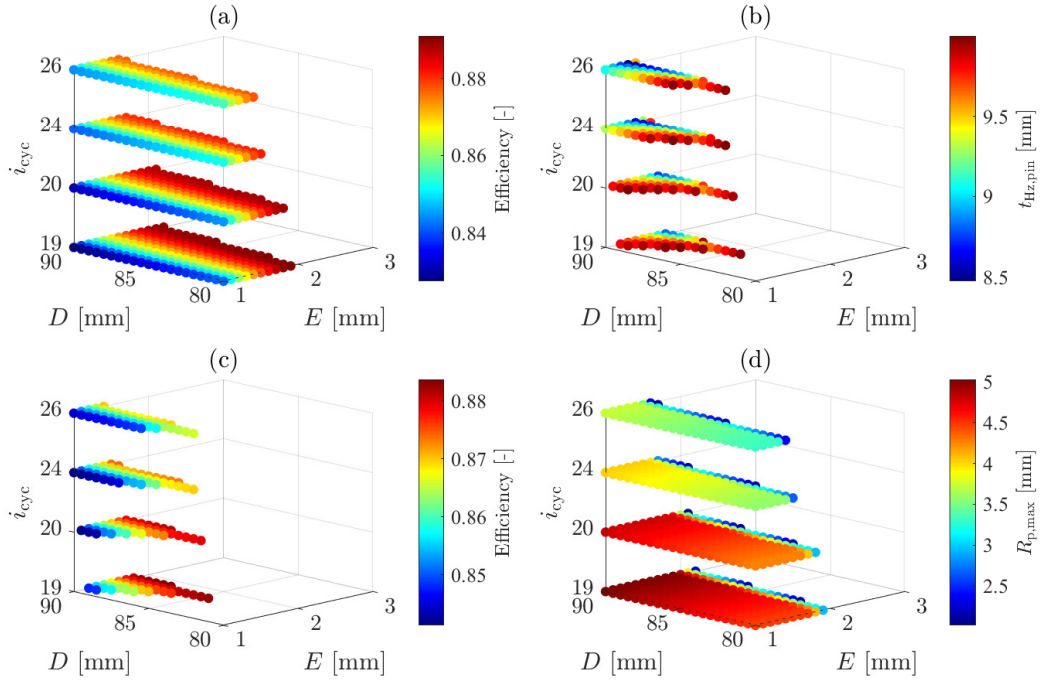


**Figure 2.** (**a**) Efficiency values for all geometrically valid solutions. (**b**) Minimum required disk thickness (limited at 10 mm). (**c**) Efficiency of all solutions satisfying the thickness constraint. (**d**) Pin radius adopted for every solution.

Once the geometry of the disk profile is defined, the geometry of the output holes and rollers should be determined. Similarly to the first optimization, the efficiency behavior is studied varying rollers' pitch diameter $D_{out}$, diameter $D_{roll}$, and number $N_{or}$.

Hertz theory is also applied to the contact points between disk and rollers to compute minimum thickness $t_{Hz,out}$, Figure 3b. For the sizing of the output rollers, the bending resistance is also taken into account, which results in a maximum length of the rollers, strictly related to the maximum thickness of the disk $t_{bend}$ shown in Figure 3c. The condition to be respected in this case is $t_{Hz,out} < 10\,mm < t_{bend}$. Between all compliant solutions, shown in Figure 3d, the most efficient is selected, completing the design procedure of the cycloidal drive.

### *3.2. Cycloidal Stage Design Results*

Following the described optimization process, the cycloidal stage geometry is set. The main parameters and their final value are summed up in Table 2, while the obtained 2D drawing is shown in Figure 4. In this configuration, the estimated efficiency of the cycloidal stage reaches 90%.

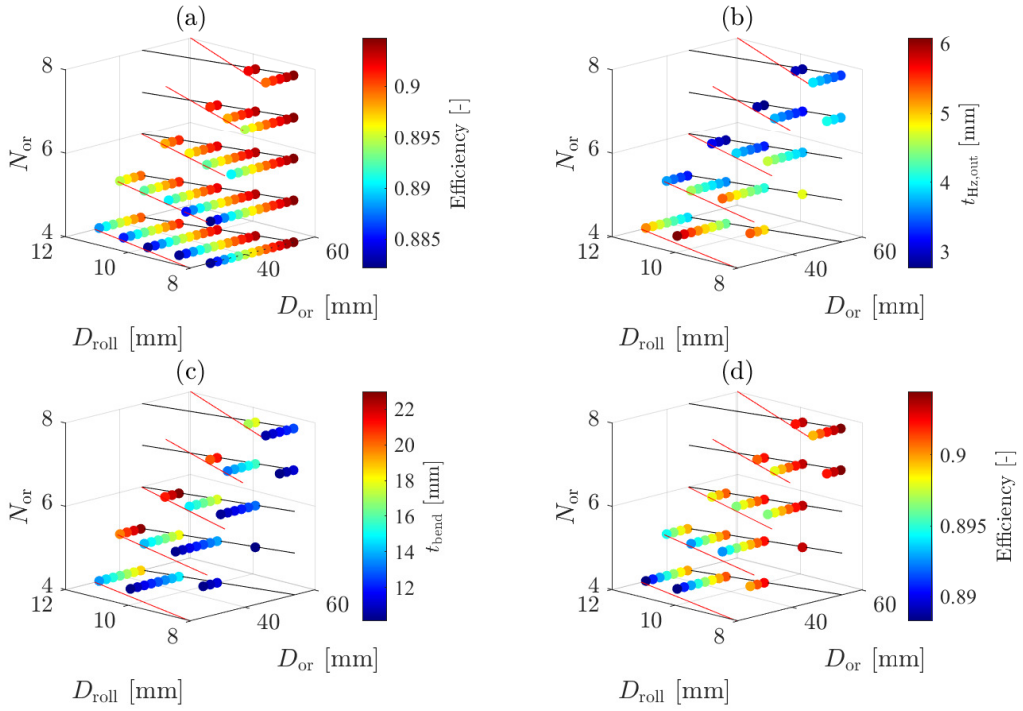


**Figure 3.** (**a**) Efficiency values for all geometrically valid solutions. (**b**) Minimum required disk thickness due to Hertzian contact. (**c**) Maximum allowable disk thickness due to rollers bending. (**d**) Efficiency of all solutions satisfying both thickness constraints. Red and black lines indicate, respectively, output holes interference limit and minimum clearance from disk profile.

**Table 2.** Cycloidal drive optimized design parameters.

| Description | Symbol | Value | Unit |
|---|---|---|---|
| Transmission ratio | $i_{cyc}$ | 19 | – |
| Disk thickness | $t$ | 10 | mm |
| Fixed pins pitch diameter | $D$ | 85 | mm |
| Fixed pins radius | $R_p$ | 4 | mm |
| Eccentricity | $E$ | 1.7 | mm |
| Output holes number | $N_{or}$ | 8 | – |
| Output holes pitch diameter | $D_{or}$ | 54 | mm |
| Output rollers diameter | $D_{roll}$ | 8 | mm |

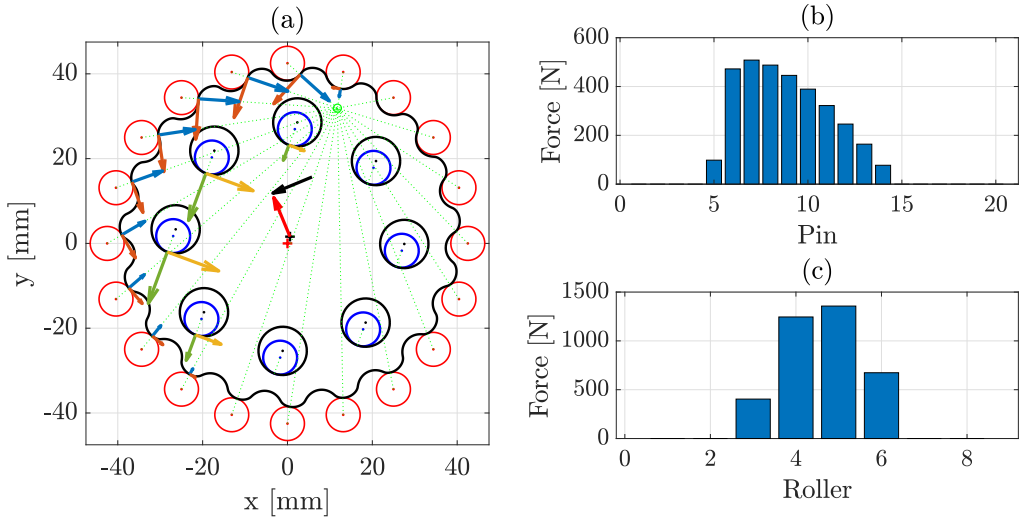


**Figure 4.** Cycloidal disk final design. (**a**) Multibody model; arrows denote force components at the contact points. Contact forces (**b**) between disk and pins, and (**c**) between lobes and output rollers.

https://doi.org/10.3390/engproc2026131021

## 4. Polymer-Based Planetary Drive

Once the design of the low-speed cycloidal stage is completed and its gear ratio fixed, the high-speed stages requirements are defined. As previously explained in Section 2, the aim is to keep $i_{tot} \approx 87$ and to maintain the same ratio for both planetary and magnetic stages. Through the optimization process, the cycloidal stage ratio is fixed $i_{cyc} = 19$ leading to a fast-stage ratio of $i_{st2} = 4.66$, as from Equations (1) and (2).

The configuration exploited for the planetary stage is depicted in Figure 5. The ring of the planetary stage is fixed, input shaft from the electric machine is connected to the sun gear, while the carrier is connected to the eccentric input shaft of the cycloidal stage. The envelope constraint for the ring gear is set to the same diameter of 85 mm previously adopted for the fixed pins of the cycloidal drive, to achieve compactness of the overall gearbox design.

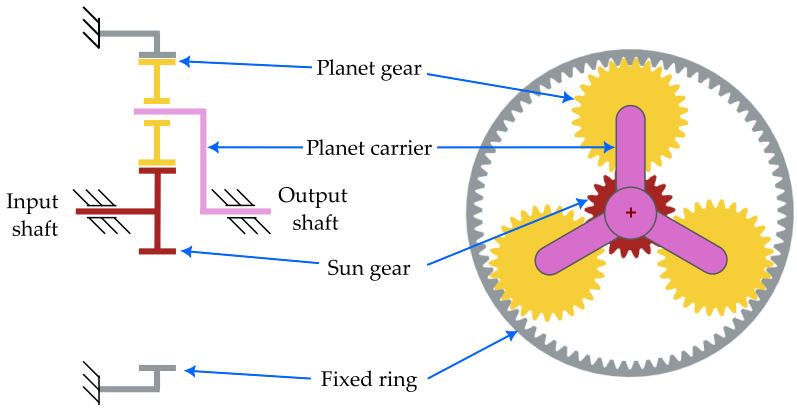


**Figure 5.** Planetary drive architecture.

High strength polymer gears offer many advantages with respect to standard steel gears, and are replacing them in various applications, also in the automotive field [16]. They can provide weight reduction, cost-effective production especially when injection molding is exploited, low friction and wear, and of course improved NVH characteristics [17].

Between the various polymers that can be adopted, Poly-ether ether ketone (PEEK) can offer a good balance between mechanical characteristics and NVH performances. It presents an higher heat deflection temperature (HDT) with respect to engineering plastics like POM and PA [18], meaning PEEK can withstand higher mechanical loads at higher temperatures.

Static sizing of the gears is carried out following normative VDI 2736, selecting not reinforced PEEK, exploiting the commercial software KISSsoft®. The main parameters of the adopted planetary design are reported in Table 3.

**Table 3.** PEEK planetary stage design parameters.

| Description | Symbol | Value | Unit |
|---|---|---|---|
| Transmission ratio | $i_{st2}$ | 4.66 | – |
| Facewidth | $b$ | 10 | mm |
| Gear module | $m$ | 1 | mm |
| Pressure angle | $\alpha$ | 20 | deg |
| Number of teeth | $[z_{sun}, z_{pl}, z_{ring}]$ | [21, 28, 77] | – |

## 5. Magnetic Drive

Magnetic gearboxes (MGs) are transmission systems in which the coupling between high-speed and low-speed rotors is not determined by the exchange of contact forces, as in mechanical gearboxes, but by the interaction of the harmonics of the magnetic field.

Their contactless nature enables minimal wear and low maintenance. This feature is also advantageous in applications where low noise emissions are paramount.

Torque transmission capability is greatly enhanced by the addition of the so-called modulator teeth. These blocks focus the magnetic flux generated by the magnets, thereby reducing dispersion and maximizing torque transmission. The most common design remains the radial architecture proposed by Atallah and Howe [19], with two concentric rotors and a modulator between them, as shown in Figure 6.

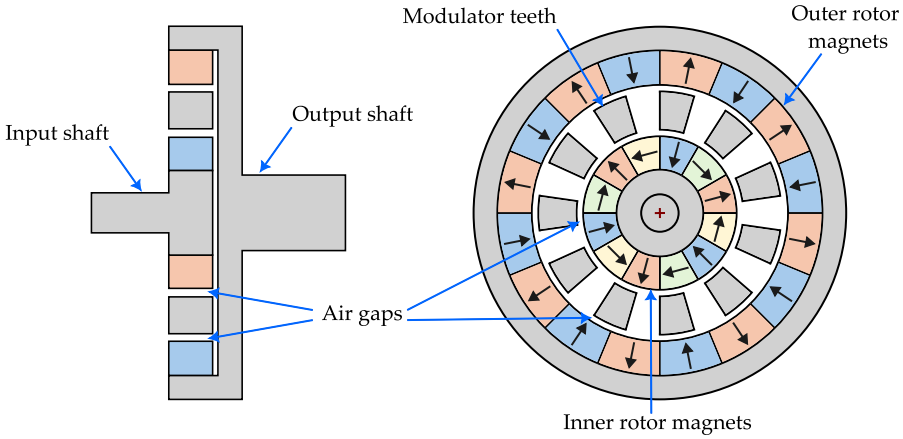


**Figure 6.** Studied magnetic gear structure. Arrows in the magnets indicate their polarization direction. The inner rotor shows a Halbach magnetization pattern.

To further increase the volumetric torque density ($VTD$) of magnetic gearboxes, Halbach magnetization patterns can be introduced, as shown in Figure 6 for the inner rotor. This allows for a more sinusoidal flux distribution and a stronger interaction among magnetic field harmonics [20].

*Magnetic Stage Design Results*

In the present work, the design of the MG stage was performed using a genetic algorithm. The two-dimensional geometry of the gearbox was parametrized in MATLAB R2025a and transferred to the software Finite Element Method Magnetics (FEMM). The model implemented a static torque computation to evaluate the maximum torque capability of each design. Iron losses useful to map the transmission efficiency were quantified through the Bertotti equation [21].

The optimization phase was carried out using MATLAB, and setting the volumetric torque density of the system as the objective function to be maximized. The addition of the efficiency to the optimization was deemed not necessary, as it increased the computational burden while not giving significant advantages in terms of power loss reduction.

To start the optimization process, the main requirements for the MG are fixed. Transmission ratio is fixed at $i_{st2} = 4.66$ after the optimization of the cycloidal drive led to a ratio $i_{cyc} = 19$, as already pointed out in Section 4. The outer radius $R_o = 45\,\text{mm}$ matches the previously existing benchmark planetary gearbox. The axial length $L = 20\,\text{mm}$ represents an upper limit to preserve compactness. The maximum outer rotor torque was limited as well to the value of 15 Nm, as higher torques would make the system unnecessarily bulky, while not providing useful improvements, considering the requirements of the application.

The equations determining the gear ratio and the necessary number of modulator poles of a magnetic gearbox are

$$i_{st2} = -\frac{N_o}{N_i} \tag{5}$$

$$N_p = N_o + N_i \tag{6}$$

where $N_i$ represents the number of pole pairs on the inner rotor, $N_o$ is the number of pole pairs on the outer rotor and $N_p$ the number of modulator poles. To obtain the established value of gear ratio, values were set to $N_i = 3$, $N_o = 14$, and $N_p = 17$.

The variables to be optimized are the axial length of the mechanism $L$, the inner and outer rotor permanent-magnet thickness $t_{pmi}$ and $t_{pmo}$, the inner and outer rotor iron yoke thickness $t_i$ and $t_o$ and the stator modulator poles thickness $t_p$.

Following its torque improvement, a Halbach array was implemented in the inner rotor, where the amount of poles is low. Instead, a regular array with two segments per pole was used on the outer rotor, where the magnets are higher in number. A preliminary analysis demonstrated that this hybrid design performs 8.46% better than the case with regular arrays on both rotors in terms of maximum torque density. By converse, exploiting Halbach arrays on both rotors improves the maximum torque output by 19.44% when compared to the hybrid design. Despite exhibiting the highest torque transmission capability, the Halbach configuration presents a large number of magnetic pole pieces with limited dimensions, which would represent an important drawback in terms of assembly. Therefore, the hybrid configuration was selected. Figure 7 shows the comparison between the outer rotor torque varying the torque angle of the three studied designs, with fixed parameters.

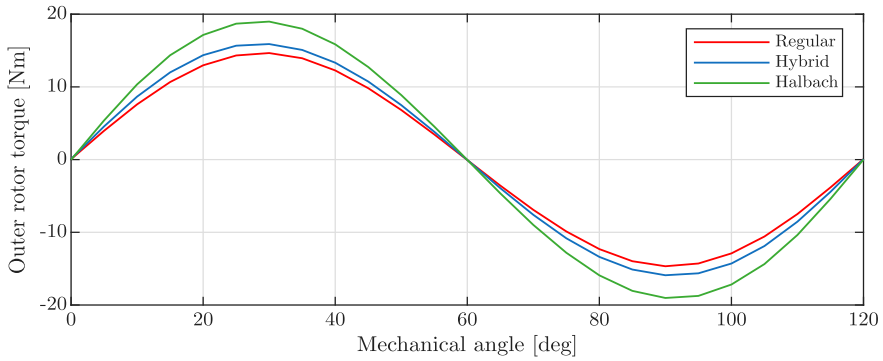


**Figure 7.** Transmitted torque at the outer rotor as a function of its mechanical angle for three different permanent-magnet configurations: conventional arrays (red), Halbach arrays (green), hybrid arrays (blue).

Table 4 lists the resulting parameters and performance metrics of the transmission torque optimization. In Figure 8a, a simulation of the final geometry in FEMM is shown. Figure 8b presents the efficiency map obtained by collecting the performance of the magnetic gear transmission in multiple working points of the torque-speed plane.

To account for flux leakage end effects, the performance of the designed magnetic gearbox was evaluated with a 3D finite-element model. As detailed in [22], end effects may cause a significant reduction of the torque capability, especially for relatively short designs like the one presented in this work ($D/L = 7.5$). Since the entity of the overestimation using 2D models can reach up to 40%, the need of a 3D model is evident. In this study, the software Ansys Maxwell was used to reproduce the 3D configuration. The maximum achievable value of transmitted torque at the outer rotor for the studied design drops from 15.84 Nm in the 2D simulation to 11.51 Nm in 3D, with a reduction of 27.84% , aligned with

literature data. Still, the reached peak torque satisfies the requirement of the actuator. The same performance decrease is, of course, visible in the value of $VTD$. Figure 9 shows the behavior of the inner and outer rotor torque over a full electrical period, comparing the 2D and 3D results.

**Table 4.** Optimization variable final values.

| Description | Symbol | Value | Unit |
|---|---|---|---|
| Gearbox axial length | $L$ | 12 | mm |
| Inner rotor PM thickness | $t_{\mathrm{pmi}}$ | 14.2 | mm |
| Outer rotor PM thickness | $t_{\mathrm{pmo}}$ | 5 | mm |
| Inner rotor yoke thickness | $t_{\mathrm{i}}$ | 6.6 | mm |
| Outer rotor yoke thickness | $t_{\mathrm{o}}$ | 5 | mm |
| Stator modulators thickness | $t_{\mathrm{p}}$ | 5.6 | mm |
| Outer diameter | $D$ | 90 | mm |
| Volumetric torque density | $VTD$ | 208.13 | kNm/m$^3$ |
| Maximum inner rotor torque | $T_{\mathrm{imax}}$ | 3.37 | Nm |
| Maximum outer rotor torque | $T_{\mathrm{omax}}$ | 15.89 | Nm |

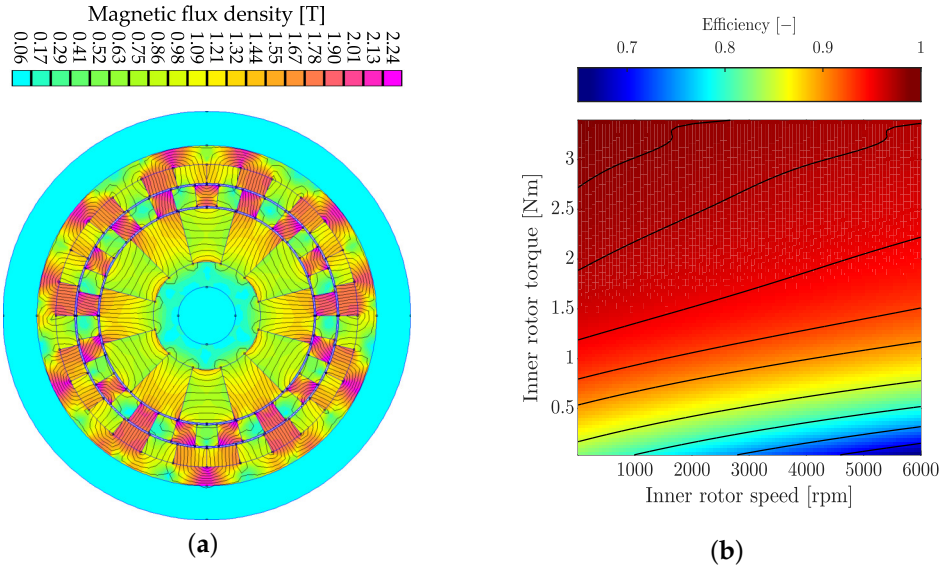


**Figure 8.** (**a**) Finite-element simulation of the final configuration of the magnetic gear transmission. (**b**) Efficiency map in the torque-speed plane.

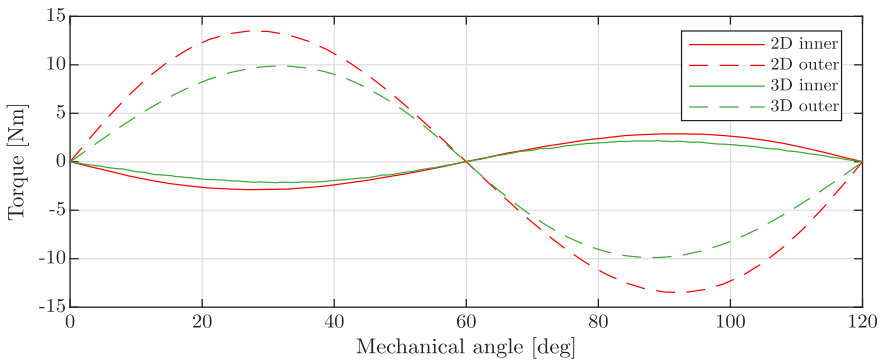


**Figure 9.** Transmitted torque at the inner (dashed) and outer (solid) rotors as a function of its mechanical angle using 2D models in FEMM (red) and 3D models in Ansys Maxwell (green).

## 6. Discussion and Conclusions

The expected features of the two proposed designs can be compared against the benchmark steel planetary gearbox, as shown in Table 5. Both compound reducers show satisfactory efficiency, slightly decreased with respect to the benchmark, but still suitable for the effectiveness of the active suspension system. Torque density is also comparable, packaging constraints are satisfied and compactness of the actuator is preserved.

**Table 5.** Comparison between packaging and efficiency characteristics of the final proposed designs and the benchmark transmission.

| Parameter | Benchmark Planetary | Cycloidal + Polymer Planetary | Cycloidal + Magnetic Stage |
|---|---|---|---|
| Estimated average efficiency | ∼90% | ∼80% | ∼85% |
| Gearbox axial length $L$ | 20 mm | 30 mm | 32 mm |
| External active diameter $D$ | 85 mm | 85∼90 mm | 90 mm |

In conclusion, this paper explored alternative transmission solutions for rotary electromagnetic shock absorbers. A cycloidal stage was combined with a polymer-based planetary stage or a magnetic gear stage. The proposed solutions were compared against a benchmark planetary gearbox for the intended application. As expected, efficiency and compactness were slightly penalized in the new designs. These performance reductions were quantified numerically through detailed models. Nevertheless, the new topologies appear promising in terms of noise, as they implement technologies, materials and methods that involve significantly lower acoustic emissions. Future works and developments will focus on the manufacturing and testing of the new prototypes to experimentally assess their energetic and NVH features and have a direct comparison with the benchmark actuator.

**Author Contributions:** Conceptualization, R.G. and N.A.; methodology, G.M., G.B., G.S. and X.Z.; software, G.M., G.B. and X.Z.; validation, G.M., G.B., G.S. and X.Z.; formal analysis, G.M., G.B. and G.S.; investigation, G.M., G.B. and X.Z.; resources, N.A.; data curation, G.M., G.B. and X.Z.; writing—original draft preparation, G.M., G.B. and X.Z.; writing—review and editing, G.S. and R.G.; visualization, G.M., G.B. and R.G.; supervision, R.G. and N.A.; project administration, N.A.; funding acquisition, N.A. All authors have read and agreed to the published version of the manuscript.

**Funding:** This research was partially funded by the European Commission under grants no. 101138110 (SmartCorners project). G. Bisciaio carried out this study within the project PNRR-NGEU, which has received funding from the MUR–DM 117/2023.

**Institutional Review Board Statement:** Not applicable.

**Informed Consent Statement:** Not applicable.

**Data Availability Statement:** The original contributions presented in this study are included in the article. Further inquiries can be directed to the corresponding author.

**Conflicts of Interest:** The authors declare no conflicts of interest.

## References

1. Abdelkareem, M.A.; Xu, L.; Ali, M.K.A.; Elagouz, A.; Mi, J.; Guo, S.; Liu, Y.; Zuo, L. Vibration energy harvesting in automotive suspension system: A detailed review. *Appl. Energy* **2018**, *229*, 672–699. [CrossRef]
2. Tonoli, A.; Amati, N.; Detoni, J.G.; Galluzzi, R.; Gasparin, E. Modelling and validation of electromechanical shock absorbers. *Veh. Syst. Dyn.* **2013**, *51*, 1186–1199. [CrossRef]
3. Willems, M. Wheel Suspension for a Motor Vehicle. U.S. Patent 8,573,604, 5 November 2013.
4. Galluzzi, R.; Circosta, S.; Amati, N.; Tonoli, A. Rotary regenerative shock absorbers for automotive suspensions. *Mechatronics* **2021**, *77*, 102580. [CrossRef]

5. Wellmann, T.; Tousignant, T.; Govindswamy, K.; Tomazic, D.; Steffens, C.; Janssen, P. *NVH Aspects of Electric Drive Unit Development and Vehicle Integration*; SAE Technical Paper 2019-01-1454; SAE International: Warrendale, PA, USA, 2019.
6. Sensinger, J.W. Efficiency of high-sensitivity gear trains, such as cycloid drives. *J. Mech. Des.* **2013**, *135*, 071006. [CrossRef]
7. Shoaei, A.; Wang, Q. A comprehensive review of concentric magnetic gears. *IEEE Trans. Transp. Electrif.* **2023**, *10*, 5581–5598. [CrossRef]
8. Kapelevich, A. *High Gear Ratio Epicyclic Drives Analysis*; Technical report; AKGears, LLC: Alexandria, VA, USA, 2014.
9. Machine Design. Planetary Gear Ratios, 2000. Available online: https://www.machinedesign.com/archive/article/21828399/planetary-gear-ratios (accessed on 10 September 2025).
10. Jing, L.; Huang, Z. The Effect of Number of Pole Pairs on Torque Ripple of Magnetic Gear. *Prog. Electromagn. Res. M* **2019**, *86*, 115–123. [CrossRef]
11. Praslicka, B.; Gardner, M.C.; Johnson, M.; Toliyat, H.A. Review and analysis of coaxial magnetic gear pole pair count selection effects. *IEEE J. Emerg. Sel. Top. Power Electron.* **2021**, *10*, 1813–1822. [CrossRef]
12. Sensinger, J.W.; Lipsey, J.H. Cycloid vs. harmonic drives for use in high ratio, single stage robotic transmissions. In *Proceedings of the 2012 IEEE International Conference on Robotics and Automation*; IEEE: Piscataway, NJ, USA, 2012; pp. 4130–4135.
13. Lee, K.; Hong, S.; Oh, J.H. Development of a lightweight and high-efficiency compact cycloidal reducer for legged robots. *Int. J. Precis. Eng. Manuf.* **2020**, *21*, 415–425. [CrossRef]
14. Blanche, J.; Yang, D. Cycloid Drives With Machining Tolerances. *J. Mech. Transm. Autom. Des.* **1989**, *111*, 337–344. [CrossRef]
15. Sensinger, J.W. Unified Approach to Cycloid Drive Profile, Stress, and Efficiency Optimization. *J. Mech. Des.* **2010**, *132*. [CrossRef]
16. Kilian, P.; Kuhmann, K. Getting to the heart of wheels – designing quieter, more energy efficient gears with PEEK. *Kunststoffe Int.* **2022**, *5*, 58–61.
17. Zorko, D.; Kalister, R.; Černe, B. An investigation on the NVH performance of plastic gears. *Forsch. Ingenieurwesen* **2025**, *89*, 128. [CrossRef]
18. Kilian, P.; Kuhmann, K. Applications of PEEK gears for high-power transmissions. In *Polymer Gears*; Elsevier: Amsterdam, The Netherlands, 2025; pp. 667–677.
19. Atallah, K.; Howe, D. A novel high-performance magnetic gear. *IEEE Trans. Magn.* **2002**, *37*, 2844–2846. [CrossRef]
20. Jian, L.; Chau, K. A coaxial magnetic gear with Halbach permanent-magnet arrays. *IEEE Trans. Energy Convers.* **2010**, *25*, 319–328. [CrossRef]
21. Bertotti, G. General properties of power losses in soft ferromagnetic materials. *IEEE Trans. Magn.* **1988**, *24*, 621–630. [CrossRef]
22. Gerber, S.; Wang, R. Analysis of the end-effects in magnetic gears and magnetically geared machines. In *Proceedings of the 2014 International Conference on Electrical Machines (ICEM)*; IEEE: Piscataway, NJ, USA, 2014; pp. 396–402.


**Disclaimer/Publisher's Note:** The statements, opinions and data contained in all publications are solely those of the individual author(s) and contributor(s) and not of MDPI and/or the editor(s). MDPI and/or the editor(s) disclaim responsibility for any injury to people or property resulting from any ideas, methods, instructions or products referred to in the content.